Defect processes in Li2ZrO3: insights from atomistic modelling

Kordatos, A, Christopoulos, S-RG, Kelaidis, N & Chroneos, A

Original citation:
Kordatos, A, Christopoulos, S-RG, Kelaidis, N & Chroneos, A 2017, 'Defect processes in Li2ZrO3: insights from atomistic modelling' *Journal of Materials Science: Materials in Electronics*, vol (in press), pp. (in press)
http://dx.doi.org/10.1007/s10854-017-6984-5

DOI 10.1007/s10854-017-6984-5
ISSN 0957-4522
ESSN 1573-482X

Publisher: Springer

J Mater Sci: Mater Electron
DOI 10.1007/s10854-017-6984-5

Defect processes in Li_2ZrO_3: insights from atomistic modelling

A. Kordatos[1] · S.-R. G. Christopoulos[1] · N. Kelaidis[1] · A. Chroneos[1,2]

Received: 25 March 2017 / Accepted: 17 April 2017

Abstract Lithium zirconate (Li_2ZrO_3) is an important material that is considered as an anode in lithium-ion batteries and as a nuclear reactor breeder material. The intrinsic defect processes and doping can impact its material properties. In the present study we employ density functional theory calculations to calculate the defect processes and doping in Li_2ZrO_3. Here we show that the lithium Frenkel is the dominant intrinsic defect process and that dopants substituting in the zirconium site strongly associate with oxygen vacancies. In particular, it is calculated that divalent dopants more strongly bind with oxygen vacancies, with trivalent dopants following in binding energies and even tetravalent dopands having significant binding energies. The results are discussed in view of the application of Li_2ZrO_3 in energy applications.

1 Introduction

Li_2ZrO_3 is a material that has been used or considered for numerous applications including anode in lithium ion batteries [1], solid sorbent for reversible capture of CO_2 [2–6], ceramic breeder for helium-cooled pebble bed blankets in reactors [7–10], as well as a coating for anodes and cathodes [11, 12]. Energy storage applications require a high Li diffusion coefficient and a stable electrochemical performance. In a recent study, Ferreira et al. [13] employed density functional theory (DFT) simulations in conjunction with experimental nuclear magnetic resonance (NMR) in order to investigate the Li ion migration mechanisms. Disorder in the anion sublattice can impact the material properties and the diffusion of point defects [14, 15]. This is a common future in energy related materials where intrinsic disorder and doping can influence the formation (i.e. concentration of point defects mediating diffusion) and the migration (i.e. the energy barriers for diffusion) [16–19]. Controlling point defects such as vacancies is important for semiconductors, superconductors, and oxides [20–28]. A way to defect engineer the concentration and clustering of point defects in the anion sublattice (for example oxygen vacancies) is via the introduction of dopants. This is effectively to maintain charge balance in the lattice [29]. For example the introduction of two trivalent dopants in the tetravalent cerium site in CeO_2 can be charge balanced by the formation of an oxygen vacancy. Therefore the introduction of trivalent dopants in CeO_2 is an efficient way to form oxygen vacancies at concentrations higher than the equilibrium concentration [29].

Atomistic simulation is an efficient and powerful way to understand the energetics of point defects in energy materials [30–32]. The main aim of the present study is to systematically investigate the intrinsic defect processes and impact of doping in Li_2ZrO_3 using DFT. In particular, we consider here divalent (Mg, Zn, Ca, Cd, Sr, Ba), trivalent (Al, Ga, Sc, In, Y) and tetravalent (Si, Ge, Ti, Sn, Pb, Ce) substitutionals and their association with oxygen vacancies.

✉ A. Chroneos
alexander.chroneos@imperial.ac.uk

[1] Faculty of Engineering, Environment and Computing, Coventry University, Priory Street, Coventry 1 5FB, UK

[2] Department of Materials, Imperial College London, London 7 2AZ, UK

Published online: 26 April 2017

2 Methodology

2.1 Crystallography

Li_2ZrO_3 is monoclinic within the C2/c space group (space group number 15) with lattice parameters a = 5.422, b = 9.022 and c = 5.419 Å (unit cell volume 244.5 $Å^3$) and β = 112.71° [33]. In the 24 atom unit cell there are two non-equivalent Li^+ ions and two Zr^{4+} residing at the Oc and 4e Wyckoff positions, whereas the O^{2-} ions reside in the 4d and 8f positions. A schematic representation of the Li_2ZrO_3 unit cell is given in Fig. 1a.

2.2 Density functional theory

In the present study we employ plane wave DFT code CASTEP [34, 35]. Exchange and correlation interactions were formulated with the corrected density functional of Perdew, Burke and Ernzerhof (PBE) [36], within the generalized gradient approximation (GGA) in conjunction with ultrasoft pseudopotentials [37]. The plane wave basis set was set to a cut-off of 400 eV. A 4 × 2 × 4 Monkhorst–Pack (MP) [38] k-point grid was used with a 96 atomic site supercell. All the calculations were under constant pressure conditions. Convergence was tested by increasing the cut-off up to 800 eV, the MP grid to 2 × 2 × 2 and by considering up to 4 × 2 × 4. These resulted in energy changes of less than 0.01 eV.

3 Results and discussion

3.1 Intrinsic defect processes

The energetics of Frenkel defects are important when considering point defect related processes (for example diffusion) in energy materials. Additionally, in nuclear applications a low pair formation energy can be associated with a higher concentration of persistent defects that can lead to the loss of the material crystal structure. In that respect radiation damage can be visualized as an accumulation of defects formed by displacement cascades [39, 40]. The three key Frenkel reactions in Kröger–Vink notation (for example in this notation V''''_{Zr} and $Zr_i^{\cdot\cdot\cdot\cdot}$ will denote a vacant Zr site and a Zr interstitial defect respectively) [41] are

$$Zr_{Zr}^{x} \rightarrow V''''_{Zr} + Zr_i^{\cdot\cdot\cdot\cdot} \quad (1)$$

$$Li_{Li}^{x} \rightarrow V'_{Li} + Li_i^{\cdot} \quad (2)$$

$$O_O^{x} \rightarrow V_O^{\cdot\cdot} + O_i'' \quad (3)$$

The oxygen Frenkel energy (Eq. 3) was calculated to be 7.35 eV, which is reasonably high. Concerning the cation Frenkel energies it is calculated that the Li Frenkel energy is significantly lower (5.77 eV) as compared to the Zr Frenkel energy (19.56 eV). In a sense these Frenkel defect formation energies reflect that it is energetically unfavourable to introduce highly charged defects (for example $Zr_i^{\cdot\cdot\cdot\cdot}$) in the Li_2ZrO_3 lattice.

This is also the case for the formation of Schottky and antisite defects. The formation of Schottky defects in Li_2ZrO_3 is given by:

$$2Li_{Li}^{x} + Zr_{Zr}^{x} + 3O_O^{x} \rightarrow 2V'_{Li} + 2V''''_{Li} + 3V_O^{\cdot\cdot} \quad (4)$$

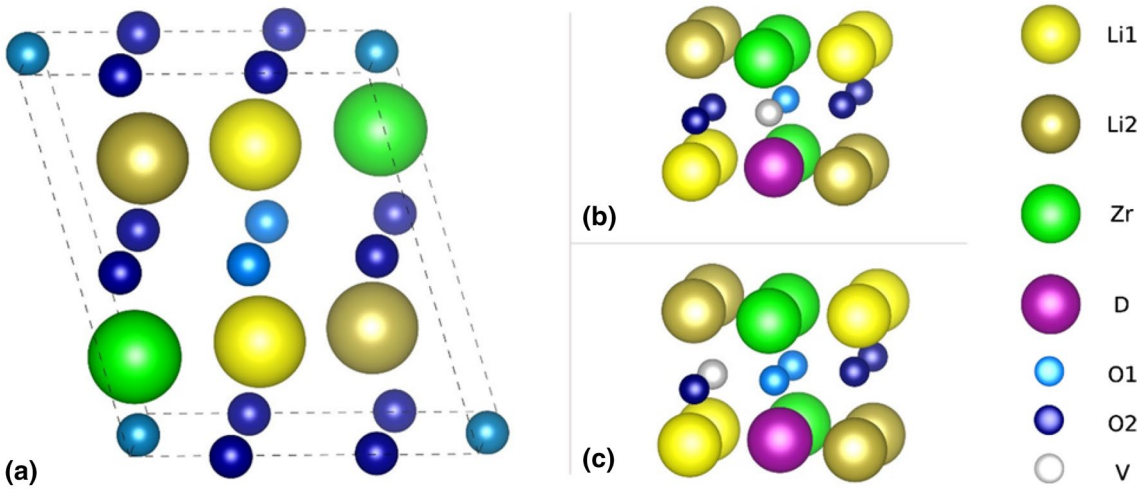

Fig. 1 A schematic representation of **a** the monoclinic Li_2ZrO_3 unit cell (lattice parameters a = 5.422, b = 9.022 and c = 5.419 Å), **b** the Dopant − $V_O^{\cdot\cdot}$ defect cluster for a $V_O^{\cdot\cdot}$ at the O1 site and **c** the Dopant − $V_O^{\cdot\cdot}$ defect cluster for a $V_O^{\cdot\cdot}$ at the O2 site

The Schottky defect formation is calculated to be 28.55 eV.

In the process of radiation damage the point defects formed can recombine or occupy an alternative lattice site to form an antisite defect [40]. Low antisite formation energies imply that a substantial concentration of residual defects will be present in the material [42]. The antisite formation mechanisms are given by:

$$Zr^{x}_{Zr} + Li^{x}_{Li} \rightarrow Zr^{\cdots}_{Li} + Li'''_{Li} \quad (5)$$

$$Zr^{x}_{Zr} + O^{x}_{O} \rightarrow Zr^{\cdots\cdots}_{O} + O''''''_{Zr} \quad (6)$$

$$Li^{x}_{Li} + O^{x}_{O} \rightarrow Li^{\cdots}_{O} + O'''_{Li} \quad (7)$$

It is calculated here that the antisite defect energies are substantial (12.88 eV for Eq. 5; 23.35 eV for Eq. 6; 12.59 eV for Eq. 7). In addition, it is logical that Eq. 6 is the most energetically unfavourable case as it displays the highest difference in effective charges (i.e. the Zr^{4+} will not be accommodated in a O^{2-} position and vice versa). Even the other energies from Eq. 5 and Eq. 6 (above 12 eV) lead to very high formation energy values and this in turn implies that the total concentration of antisites in Li_2ZrO_3 will be very limited.

3.2 Divalent dopants

Here we considered doping Li_2ZrO_3 with divalent dopants (M = Mg, Zn, Ca, Cd, Sr, Ba) via the relation:

$$MO \xrightarrow{Li_2ZrO_3} M''_{Zr} + V^{\cdot\cdot}_{O} + O^{x}_{O} \quad (8)$$

It can be observed by relation 8 that the introduction of divalent substitutionals in Zr sites leads to the formation of oxygen vacancies. From a physical viewpoint this is to charge balance the divalent dopant substitutional at a Zr site (M''_{Zr}) that has an effective double negative charge with an oxygen vacancy ($V^{\cdot\cdot}_{O}$) that has an effective double positive charge. Here we considered the association of M''_{Zr} with a nearest neighbour oxygen vacancy at the O1 and O2 sites (refer to Fig. 1b, c for the configurations considered here). Next nearest neighbour configurations or clusters where the two defects are further apart were calculated to be less energetically favourable.

Figure 2a represents the dependence of the binding energy with respect to the divalent dopant radius. Irrespective of the oxygen vacancy site we observe a similar trend that is the binding energies decrease with increasing dopant ionic radius (with the exception of Mg). The binding energy difference between the highest and lowest points is about 1.01 eV. Figure 2b represents the dependence of the binding energy with respect to the electronegativity of the divalent dopant. It is observed that there is an increase in binding energies as the electronegativity of the divalent dopants is increased (with the exception of Cd).

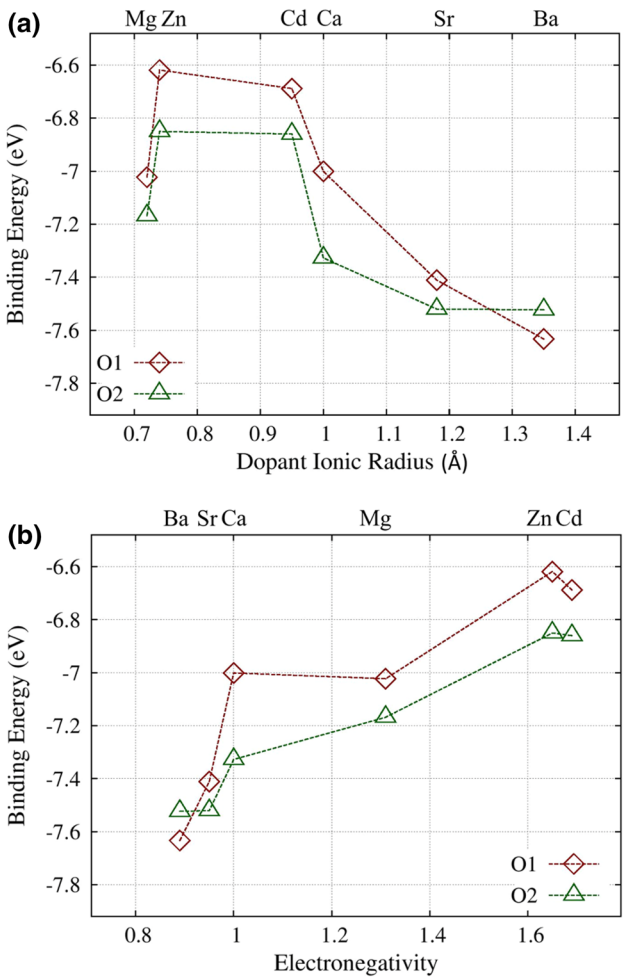

Fig. 2 Binding energies of the Dopant $-V^{\cdot\cdot}_{O}$ defect clusters with respect to **a** the divalent dopant ionic radii and **b** the electronegativity of the divalent dopant

3.3 Trivalent dopants

Considering the doping process of Li_2ZrO_3 with trivalent dopants (Al, Ga, Sc, In, Y), this will lead to the formation of one oxygen vacancy for every two trivalent atoms substituting for Zr atoms. The reaction can be described as follows:

$$R_2O_3 \xrightarrow{Li_2ZrO_3} 2R'_{Zr} + V^{\cdot\cdot}_{O} + 3O^{x}_{O} \quad (9)$$

Interestingly, defect clusters with Al and Y correspond to similar binding energies despite the fact of their radius difference of about 0.35 Å (Fig. 3a). Figure 3b corresponds to the dependence of the binding enegries with the trivalent

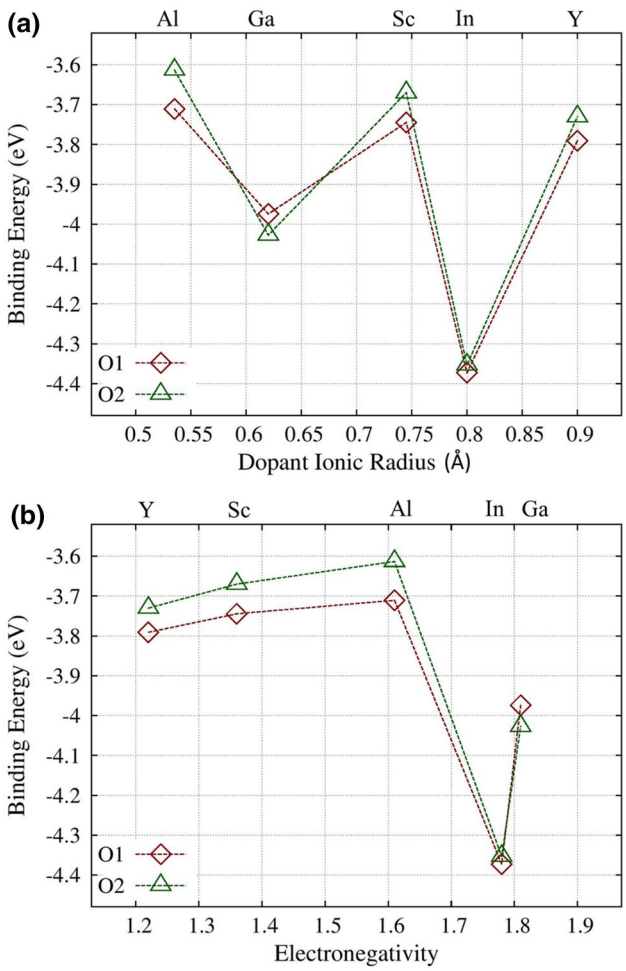

Fig. 3 Binding energies of the Dopant $-V_O^{\cdot\cdot}$ defect clusters with respect to **a** the trivalent dopant ionic radii and **b** the electronegativity of the trivalent dopant

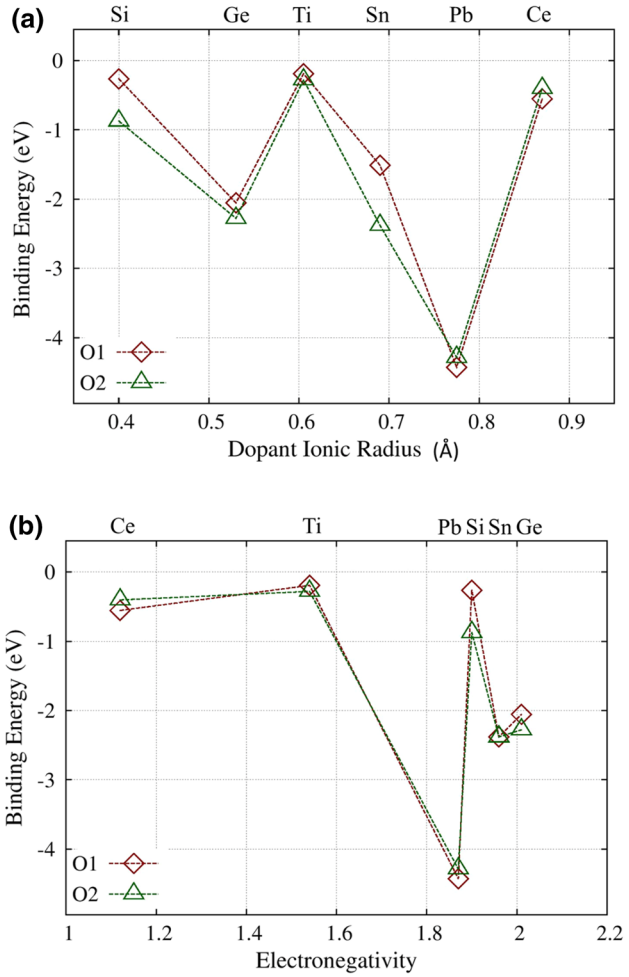

Fig. 4 Binding energies of the Dopant $-V_O^{\cdot\cdot}$ defect clusters with respect to **a** the tetravalent dopant ionic radii and **b** the electronegativity of the tetravalent dopant

dopant electronegativity and no clear trend is observed as in the case of the divalent ions.

3.4 Tetravalent dopants

Considering doping Li_2ZrO_3 with tetravalent dopants (D = Si, Ge, Ti, Sn, Pb, Ce) can also lead to an association with oxygen vacancies but this time only mainly due to the relaxation of the dopant near the oxygen vacancy. The mechanism is:

$$DO_2 \xrightarrow{Li_2ZrO_3} D_{Zr}^{x} + V_O^{\cdot\cdot} + 2O_O^{x} \quad (10)$$

As it is expected the binding energies are lower as compared to divalent and trivalent doping, where there is an element of Coulombic attraction that increase the binding energies. At any rate it is observed that the binding energies exceed a maximum of 2.4 eV, a relatively low level that reveals the weaker interaction of the dopant. However, for this particular category the dopants of maximum (Ce) and minimum (Si) radius correspond to similar binding energies (Fig. 4).

4 Summary

The present study has considered the intrinsic defect processes in Li_2ZrO_3. It is calculated that the Li Frenkel is the lowest energy and thus the dominant intrinsic defect process. Antisite defects were calculated to have very high energies and therefore it is expected that there will be only a very small concentration of antisites under most conditions.

In Li_2ZrO_3 it is energetically costly to form oxygen vacancies via the Frenkel intrinsic defect process. A way to overcome this and to form an oxygen deficient structure

is to dope with divalent or trivalent cations as these will substitute at Zr lattice sites (relations 8, 9). It is calculated here that these dopant atoms will strongly bind with nearest neighbour oxygen vacancies. For the divalent dopants the strongest association is with the largest dopants (i.e. Ca, Sr, and Ba) and this can be explained by the relaxation offered by the nearest neighbour vacancy. Tetravalent dopants will also associate with oxygen vacancies but typically with lower binding energies. At any rate doping with divalent and trivalent atoms can prove to be a defect engineering strategy to form oxygen vacancies, which is turn can be controlled by the dopants. These oxygen vacancies can have an impact on the diffusion and electronic properties of Li_2ZrO_3 and will need to be investigated in further experimental (using secondary ion mass spectrometry, XPS, NMR) and computational work.

Acknowledgements A.K. is grateful for funding from the Faculty of Engineering, Environment and Computing of Coventry university. S.-R.G.C, N.K. and A.C. are grateful for funding from the Lloyd's Register Foundation, a charitable foundation helping to protect life and property by supporting engineering-related education, public engagement and the application of research.

References

1. Y. Dong, Y. Zhao, H. Duan, J. Huang, Electrochim. Acta **161**, 219–225 (2015)
2. J. Ida, R. Xiong, Y. Lin, Sep. Purif. Technol. **36**, 41–51 (2004)
3. Q. Xiao, Y. Liu, Y. Zhong, W. Zhu, J. Mater. Chem. **21**, 3838–3842 (2011)
4. Y. Duan, Phys. Chem. Chem. Phys. **15**, 9752–9760 (2013)
5. S. Wang, C. An, Q. Zhang, J. Mater. Chem. A **1**, 3540–3550 (2013)
6. Y. Duan, J. Lekse, Phys. Chem. Chem. Phys. **17**, 22543–22547 (2015)
7. G.W. Hollenberg, J. Nucl. Mater. **123**, 896–900 (1984)
8. Y. Kawamura, M. Enoeda, K. Okuno, Fusion Eng. Des **39**, 713–721 (1998)
9. T. Kanazawa, M. Nishikawa, H. Yamasaki, K. Katayama, H. Kashimura, T. Hanada, S. Fukada, Fusion Sci. Technol. **60**, 1167–1170 (2011)
10. P. Bottke, D. Freude, M. Wilkening, J. Phys. Chem. C **117**, 8114–8119 (2013)
11. M. Thackeray, C. Johnson, J. Kim, K. Lauzze, J. Vaughey, N. Dietz, D. Abraham, S. Hackney, W. Zeltner, M. Anderson, Electrochem. Commun. **5**, 752–758 (2003)
12. X. Zhang, S. Sun, Q. Wu, N. Wan, D. Pan, Y. Bai, J. Power Sources **282**, 378–384 (2015)
13. A.R. Ferreira, K. Reuter, C. Scheurer, RSC Adv. **6**, 41015–41024 (2016)
14. D. Parfitt, A. Chroneos, A. Tarancon, J.A. Kilner, J. Mater. Chem. **21**, 2183 (2011)
15. E.E. Jay, M.J.D. Rushton, A. Chroneos, R.W. Grimes, J.A. Kilner, Phys. Chem. Chem. Phys. **17**, 178 (2015)
16. A. Kushima, B. Yildiz, J. Mater. Chem. **20**, 4809 (2010)
17. I.D. Seymour, A. Chroneos, J.A. Kilner, R.W. Grimes, Phys. Chem. Chem. Phys. **13**, 15305 (2011)
18. I.D. Seymour, A. Tarancon, A. Chroneos, D. Parfitt, J.A. Kilner, R.W. Grimes, Solid State Ionics **216**, 41 (2012)
19. D. Rupasov, A. Chroneos, D. Parfitt, J.A. Kilner, R.W. Grimes, S.Ya.. Istomin, E.V. Antipov, Phys. Rev. B **79**, 172102 (2009)
20. S. Brotzmann, H. Bracht, J. Appl. Phys. **103**, 033508 (2008)
21. A. Chroneos, J. Appl. Phys. **105**, 056101 (2009)
22. R.W. Grimes, G. Busker, M.A. McCoy, A. Chroneos, J.A. Kilner, S.P. Chen, Berich. Bunsen. Phys. Chem. **101**, 1204 (1997)
23. D. Horlait, S.C. Middleburgh, A. Chroneos, W.E. Lee, Sci. Rep. **6**, 18829 (2016)
24. S.T. Murphy, A. Chroneos, C. Jiang, U. Schwingenschlögl, R.W. Grimes, Phys. Rev. B **82**, 073201 (2010)
25. R.V. Vovk, M.A. Obolenskii, A.A. Zavgorodniy, I.L. Goulatis, V.I. Beletskii, A. Chroneos, Physica C **469**, 203 (2009)
26. R.V. Vovk, N.R. Vovk, O.V. Shekhovtsov, I.L. Goulatis, A. Chroneos, Supercond. Sci. Technol **26**, 085017 (2013)
27. E.N. Sgourou, D. Timerkaeva, C.A. Londos, D. Aliprantis, A. Chroneos, D. Caliste, P. Pochet, J. Appl. Phys. **113**, 113506 (2013)
28. A. Chroneos, R.V. Vovk, Solid State Ionics **274**, 1–3 (2015)
29. M.J.D. Rushton, A. Chroneos, S.J. Skinner, J.A. Kilner, R.W. Grimes, Solid State Ionics **230**, 37 (2013)
30. T. J. Pennycook, M. J. Beck, K. Varga, M. Varela, S. J. Pennycook, S. T. Pantelides, Phys. Rev. Lett. **104**, 115901 (2010)
31. M.J.D. Rushton, A. Chroneos, Sci. Rep. **4**, 6068 (2014)
32. D.C. Parfitt, M.W.D. Cooper, M.J.D. Rushton, S.-R.G. Christopoulos, M.E. Fitzpatrick, A. Chroneos, RSC Adv. **6**, 74018 (2016)
33. J. Hodeau, M. Marezio, A. Santoro, R. Roth, J. Solid State Chem. **45**, 170–179 (1982)
34. M.C. Payne, M.P. Teter, D.C. Allan, T.A. Arias, J.D. Joannopoulos, Rev. Mod. Phys. **64**, 1045 (1992)
35. M.D. Segall, P.J.D. Lindan, M.J. Probert, C.J. Pickard, P.J. Hasnip, S.J. Clark, M.C. Payne, J. Phys. **14**, 2717 (2002)
36. J. Perdew, K. Burke, M. Ernzerhof, Phys. Rev. Lett. **77**, 3865 (1996)
37. D. Vanderbilt, Phys. Rev. B **41**, 7892 (1990)
38. H.J. Monkhorst, J.D. Pack, Phys. Rev. B **13**, 5188 (1976)
39. J.B. Gibson, A.N. Goland, M. Milgram, G.H. Vineyard, Phys. Rev. **120**, 1229 (1960)
40. K. E. Sickafus, L. Minervini, R. W. Grimes, J. A. Valdez, M. Ishimaru, F. Li, K. J. McClellan, T. Hartmann, *Science*, **289**, 748–751 (2000)
41. F.A. Kröger, H.J. Vink, Solid State Phys. **3**, 307–435 (1956)
42. R.E. Voskoboinikov, G.R. Lumpkin, S.C. Middleburgh, Intermetallics **32**, 230–232 (2013)